

Space-charge effect of the time-varying electron injection in a diode: classical and relativistic regimes^{a)}

Yangjié Liu (刘洪杰),^{1,2, b)} Qi Tang,³ and Biyi Wu (吴比翼)^{2,4}

¹⁾*Faculty of Physics and Electronic Science, Hubei University, and Hubei Collaboration Innovation Centre for Advanced Organic Chemical Materials – Hubei Key Laboratory of Ferro & Piezoelectric Materials and Devices, 430062 Wuhan, Hubei Province, P. R. China*

²⁾*Antennas Group, School of Electrical Engineering and Computer Science, Queen Mary University of London, E1 4NS Mile End, East London, United Kingdom*

³⁾*Department of Mathematical Sciences, Rensselaer Polytechnic Institute, United States*

⁴⁾*Center for Electromagnetic Simulation, Beijing Institute of Technology, Haidian District, Beijing, P. R. China*

(Dated: compiled 2 March 2022, submitted 29 July, accepted 3 Aug 2017 to *AIP Phys. Plasmas*)

Conventionally, space-charge (SC) limited current density is defined as the maximal current density allowed to traverse a diode under a DC voltage when a time-invariant flow is injected from the cathode. In this work, we study the SC limited current density under a time-varying injection for both classical and relativistic regimes and determine the maximal amount of limited current density under certain conditions. Our simulations show that it is unlikely that a time-varying injection emitted from cathode exceeds the known SC limits, in either classical or relativistic regime.

PACS numbers: 52.59.Sa, 71.15.-m, 52.65.Rr, 68.43.Tj

^{a)} Drafted November 2016, revised 18 April 2017, POP51880 submitted 20 April, review received 1 May, revised 28 June and 16 July, POP51880A resubmitted 16 July, minor rev received 26 July, POP51880B re-resubmitted 29 July, accepted 3 Aug 2017.

^{b)} Electronic mail of corresponding author: yangjie@hubu.edu.cn

I. INTRODUCTION

It is of practical interest for plasma devices to seek enhanced density of plasma sources, which typically requires consideration of space-charge (SC) limit for a diode structure. SC limited current density describes the maximal current density allowed to transport through a diode, for a time-invariant injection from the cathode. For a diode with a gap spacing of d and a diode voltage of ϕ_g , this is known as the well-known Child-Langmuir law¹⁻³. This law extends to the more general case of nonzero initial velocity v_0 ^{4,5} and the relativistic regime⁶⁻¹⁰ when the voltage potential becomes relativistic. In recent years the efforts to achieve a higher electron flow have been very active, in both classical and relativistic regimes^{11,12}. Note that self-magnetic effect and inductive effect can both be additional factors to suppress SC limit¹².

There has been recent interest in investigating whether an injection of time-varying current density can contribute to a larger current density that is transmittable across the diode space¹³⁻²¹. On the other hand, time-varying current emission through the diode anode arises naturally even when the injection current density is *time-invariant*, with the diode voltage being fixed. For example, a recent work based on 1D charge sheet model investigated how the temporal interval becomes distorted due to space-charge effect²². Another recent work¹³ used a characteristic method to solve the 1D pressureless Euler-Poisson equations and achieved an over-classical limit by varying the anode boundary voltage with time, although the relevant characteristics are not solvable in a closed form for arbitrary temporal profiles of injection. Therefore, a general treatment for time-varying flow of electrons is demanded. In this work, we address the practical issue of time-varying injection current by solving the same 1D pressureless Euler-Poisson equations, in order to unfold the physics of time-varying injection flow of electrons. According to our simulation, it seems *unlikely* that one can transmit a time-varying injection $j(t)$ across the diode that is time-averagely higher than the conventional SC limited current density, in both classical⁴ and relativistic regimes^{8,23}. In our paper, the electrons are injected into the diode gap following the prescribed time profiles. It is assumed that SC limit is reached when reflection occurs²⁴. Then the average current densities flowing through the anode are computed and compared to the previous known SC limits. This approach is also extended to the relativistic regime⁸ when the diode voltage or the initial velocity become relativistic, and the same negative result prevails.

II. PROBLEM AND METHOD

In this section, we describe the problem of electron flow in a 1D diode structure depicted in Fig. 1 in the classical regime, and the numerical approach to determine the SC limit. They are also extended to the relativistic regime when the initial velocity becomes comparable to the speed of light, or when the relativistic diode voltage becomes comparable with the rest energy of electrons.

A. Classical regime

Consider a diode with a gap of spacing d and a fixed boundary potential difference ϕ_g between the cathode and anode. The electrons are injected from the cathode ($x = 0$) with a forced time-varying current density of $j_0(t)$ ²⁵ over a pulse length τ_p . We take the pulse length τ_p to be longer than the transit time. The 1D pressureless Euler-Poisson equations for the electron flow in a diode can be written as

$$\partial_t \rho + \partial_x(\rho v) = 0, \quad (1)$$

$$\partial_t v + v \partial_x v = \partial_x \phi, \quad (2)$$

$$\partial_x^2 \phi = \rho, \quad (3)$$

in which scaled quantities are used for position x , time t , velocity v , potential ϕ and charge density ρ similar to the previous work¹³. Note that all primed ones variables in SI units are scaled into unprimed ones to simplify the equations:

$$(x, t, v, \phi, \rho) = \left(\frac{x'}{L}, \frac{t'}{T}, \frac{v'}{L/T}, \frac{\phi'}{\Phi}, \frac{\rho'}{R} \right), \quad (4)$$

where L, T are the characteristic length and time, and the characteristic potential and density are $\Phi = mL^2/(eT^2)$, $R = \epsilon_0 \Phi / eL^2$ for simplicity¹³. An inflow boundary condition is used at $x = 0$,

$$\phi = 0, \quad v = v_0, \quad \rho(t) = \frac{J_0(t)}{v_0}, \quad 0 \leq t \leq \tau_p, \quad (5)$$

to take into account the injection current density $J_0(t)$ at the cathode $x = 0$ (see Fig. 1). Note that for a special case when $v_0 = 0$, our algorithm can deal with it with a different inflow boundary condition. More details will be elaborated in Subsec. III D. The outflow boundary condition used at $x = d$ is a fixed potential $\phi = \phi_g$.

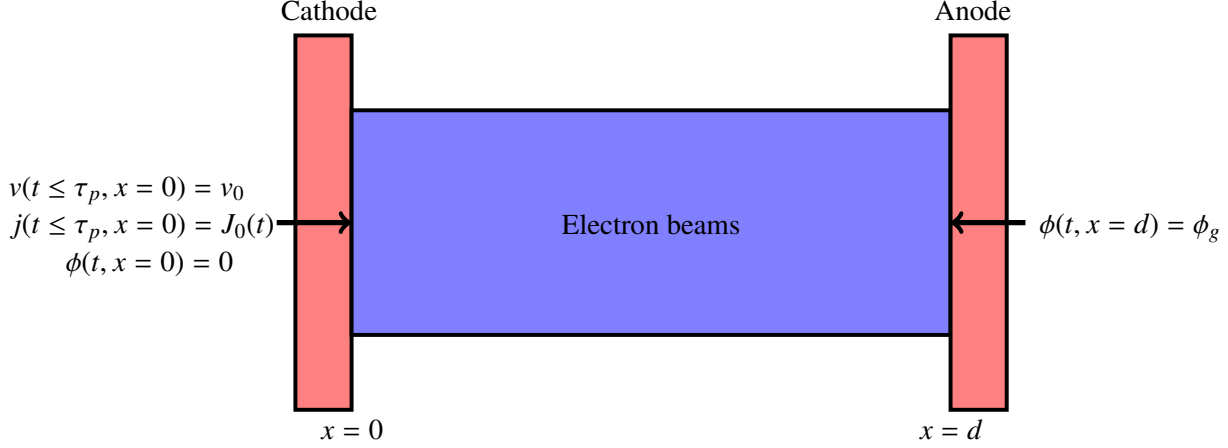


FIG. 1. Schematic: 1D diode model of voltage difference ϕ_g and spacing d . Time-dependent injection current density $J_0(t)$ up to finite time $0 \leq t \leq \tau_p$ emits from the cathode, and is dragged towards the anode with initial velocity v_0 . The blue color indicates the electron beams in the diode spacing.

The space-charge limited current density for time-invariant injection in scaled quantity can be written as^{4,13}

$$J_m = \frac{2}{9d^2} \left(v_0 + \sqrt{v_0^2 + 2\phi_g} \right)^3. \quad (6)$$

For arbitrary $J_0(t)$ at cathode, a Lax-Friedrichs scheme coupled with a second-order Poisson solver provides insight into solving the system numerically in MATLAB. In Sec. III the numerical solutions are used to observe how the charge density and diode potential along diode space d vary with time. The magnitude of the injection density is increased from small to large, and we determine that SC limit is reached when negative velocity *just* appears near cathode under injection of a certain emission profile. Here we assume that emission profile $J_0(t)$ can be expressed as

$$J_0(t) = \beta_m J_m \cdot j_m(t), \quad (7)$$

where β_m is the dimensionless magnitude and j_m is a particular time-dependent profile assumed as

follows,

$$j_0 = 1, \quad (8)$$

$$j_1 = 2\bar{t}, \quad (9)$$

$$j_2 = 3\bar{t}^2, \quad (10)$$

$$j_3 = 2(1 - \bar{t}), \quad (11)$$

$$j_4 = 3 - 3\bar{t}^2, \quad (12)$$

$$j_5 = -6\bar{t}^2 + 6\bar{t}, \quad (13)$$

$$j_6 = 12\left(\bar{t} - \frac{1}{2}\right)^2, \quad (14)$$

where the time is normalised by $\bar{t} = t/\tau_p$. Compared with other temporal profiles, these polynomial emission profiles are chosen based on the understanding that a smooth temporal function should be expanded as a series of polynomials according to Taylor series. We first choose a steady function (8), then monotonic increasing functions (9, 10), monotonic decreasing functions (11, 12), and lastly a valley function (13) and a mountain function (14)²⁶. We sweep magnitudes β_m for each m in profile $j_m(t)$ and decide the SC limit is reached when reflection *just* occurs, i.e. the velocity becomes negative, within the pulse length $0 \leq t \leq \tau_p$. As a reference when the injection flow is time-invariant $m = 0$, it is understood that β_0 should be one which corresponds to the convective SC limit J_m of Eq. (6), while other β_m 's generally differ from one.

In our simulations, we choose the electron beam length to be longer than the typical transmit time of an electron across the spacing (cf. Figs. 2-3 below). This is for the following reason. In empirical situations, one can only inject an electron beam of finite length. We thus do so in order to understand the sole role of time-dependent injection. This long pulse condition is important as when the temporal length of the electron beam becomes shorter than Child-Langmuir transmit time $3d/\sqrt{2\phi_g}$, the short-pulse limited current density can transcend Child-Langmuir limit already²⁷. Therefore we intentionally implement this long pulse condition in order to remove complication resultant from the short-pulse effect²⁷.

B. Relativistic regime

In the relativistic regime, when v_0 becomes comparable to light velocity c or the relativistic diode voltage $U := q\phi_g/mc^2 \gtrsim 0.01$, the charge density ρ become

$$\rho = \gamma\rho_0, \quad \gamma[v] := \left(1 - \frac{v^2}{\hat{c}^2}\right)^{-1/2}. \quad (15)$$

The 1D pressureless Euler-Poisson equations for relativistic electron flow are changed into

$$\partial_t \rho + \partial_x(\rho v) = 0, \quad (16)$$

$$\gamma^3(\partial_t v + v\partial_x v) = \partial_x \phi, \quad (17)$$

$$\partial_x^2 \phi = \rho. \quad (18)$$

Note that the relativistic equations are under the same scaling of Eq. (4). Therefore the light speed $\hat{c} = cT/L$. For computational purpose, let $L/T = 10^7 \text{m/s}$, so the light speed $\hat{c} = 30$ in this scale. The details of the derivation are given in Appendix A. In the relativistic regime, the space-charge limit for time-invariant injection is⁸

$$J_{\text{rm}} = \frac{c^3}{2d^2} \left[G(U, \gamma_0) \right]^2, \quad (19)$$

where $G(U, \gamma_0) := \int_0^U \left(\sqrt{(u + \gamma_0)^2 - 1} - \sqrt{\gamma_0^2 - 1} \right)^{-1/2} du$, $U := \phi_g/c^2$ and $\gamma_0 = \gamma[v_0]$. The same approach will be used to find the SC limited current density for various time profiles as in the classical case II A.

III. RESULTS

In this section, the numerical results are used to pinpoint the space-charge limit when the injection is time-varying. To assess the space-charge effect with respect to the conventional Child-Langmuir limit (6), we define two characteristic ratios: the scaled charge

$$\bar{q} := \frac{\int_0^{\tau_p} j_A(t) dt}{\int_0^{\tau_p} J_0(t) dt}, \quad (20)$$

and the scaled current density

$$\bar{j} := \frac{\int_{\tau_1}^{\tau_2} j_A(t) dt}{J_m(\tau_2 - \tau_1)}, \quad (21)$$

in which j_A represents the current density at the anode, and τ_1 and τ_2 are the starting and finishing time for j_A being positive. In the classical case $\bar{q} = 1$ indicates the critical situation that all injected charge has transmitted through the anode at the finishing time τ_p . Due to the leftover charge inside the diode, this should generally be unreachable as confirmed in Fig. 3. In the relativistic case (see (a, c, e) of Fig. 4), \bar{q} becomes larger than unity due to Lorentz length contraction²⁸. Note $\bar{j} \geq 1$ means that SC limited current density with time-varying pulse for each $j_m(t)$ profile is reached or even transcended.

A. Classical case

We first demonstrate that the output current density $j_A(t)$ at the anode is typically time-dependent, even when the injection current density is constant over the pulse. The numerical results for the case $m = 0$ are presented in Fig. 2. In Fig. 2 (a), when β_0 varies from 0.90 to 1.37, the transmitted charge at the anode (dashed line) is almost identical to the emitted charge at cathode. A careful check indicates that the smallest amount is 0.98. On the other hand in Fig. 2 (b), as β_m increases, the transmitted current density (red dashed) increases to the optimal value 89% of the SC limited one (red solid line) Eq. (6) and then goes down until 86% (blue dashed line). These observations are based on the ratios \bar{q} and \bar{j} defined in Eqs. (20) and (21). When magnitude β_0 increases more than 1.37, the whole beam starts to reflect and the space-charge limit is reached. We further study three typical cases of β_0 found from Fig. 2 (a), which are denoted in colored circles. In Fig. 2 (b) the emitted currents at the cathode (dash lines) and the transmitted currents at the anode (solid lines) of those three cases are presented in matching colors. The pulse length is chosen to be $\tau_p = 4$ in order to be longer than the time $\tau_1 = 1.15$ when the anode current becomes positive. It is concluded that even when the injection flow is time-invariant, the transmitted flow is time-dependent at the anode. Moreover, when the injection is smaller than space-charge limit (denoted as the green asterisk in Fig. 2), the transmitted current is relatively uniform in time (the black curves). When the injection is larger, the transmittance becomes damped around the central region and electrons are shaped to high values at the pulse end (see red and blue curves therein).

When the pulse length is set longer as $\tau_p = 6$, a larger current density can transmit across the anode, seen in Fig. 2 (c). Similar saturation effect due to space-charge limit is observed for the longer pulse length. The transmitted current density is extended in the central part of the pulse, as the anode current density j_A in Fig. 2 (b, d) show. To make a fair comparison, we choose $\tau_p = 4$

in the rest classical simulations.

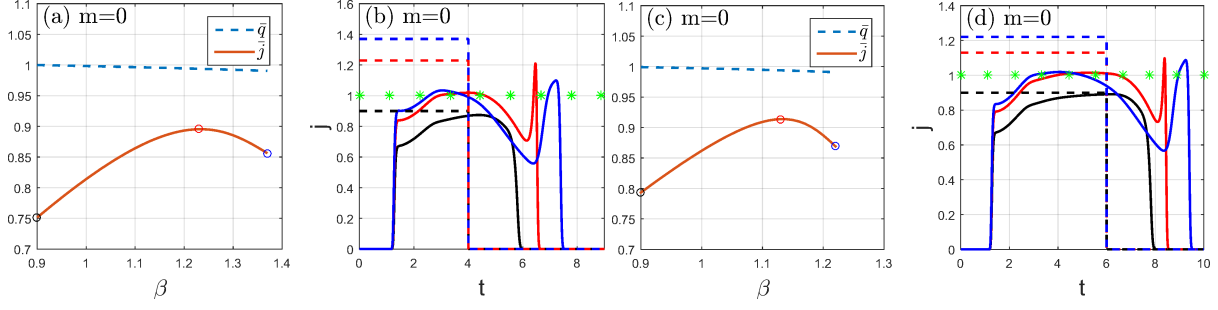


FIG. 2. (a, c) Scaled transmitted charge [cf. Eq. (20)] and scaled current density [cf. Eq. (21)]. (b, d) Transmittance profiles [solid curves, color marked according to circle marks in (a, c)] at the anode for time-invariant injection ones in classical regime. The injection profiles at the cathode are plotted in dashed curves and the SC limit in green asterisks. Parameters: $m = 0$, $v_0 = \hat{c}/60$; (a-b) $\tau_p = 4$, (c-d) $\tau_p = 6$.

Next, we study the time-varying injection of the cases $m = 1 \sim 6$. All results for six time-varying injection profiles are plotted in Fig. 3(a-l). The output density for time-varying injection is again time-varying, similar to the constant injection case before. For each m there exists an optimal magnitude β_m that the transmittance researches the maximum, closest to SC limit in Eq. 6. For example when $m = 4$ in Fig. 3 (g-h), the maximal transmittance reached at $\beta_4 = 0.54$ (in red circle) is about 90% of the space charge limit. If β_4 is larger than 0.54, the transmittance decreases. When $\beta_4 > 0.62$ (see the blue circle in Fig. 3 (h)), the electron beam starts to reflect towards the cathode and it is therefore determined that space charge limit has reached. The three cases in Fig. 3 (h) indicates that the transmittance starts to damp in the central region due to the clamping SC effect (the most pronounced for the blue curve). It shows that the SC effect dominates the time-dependent electron flow before there would be a larger current density across the diode. For all other profiles, similar clamping effects due to space charge repulsion are observed from the results. Based on these simulations, we conclude that *time-varying injection seem unlikely to contribute more than the space-charge limit (6)*. This is the main result of this paper.

B. Relativistic case

In the relativistic regime, we demonstrate that time-varying injection cannot result in a transmittance higher than its SC limit⁸. Let the anode voltage $\phi_g = 900$, and $U = \phi_g/\hat{c}^2 = 1$ so that the

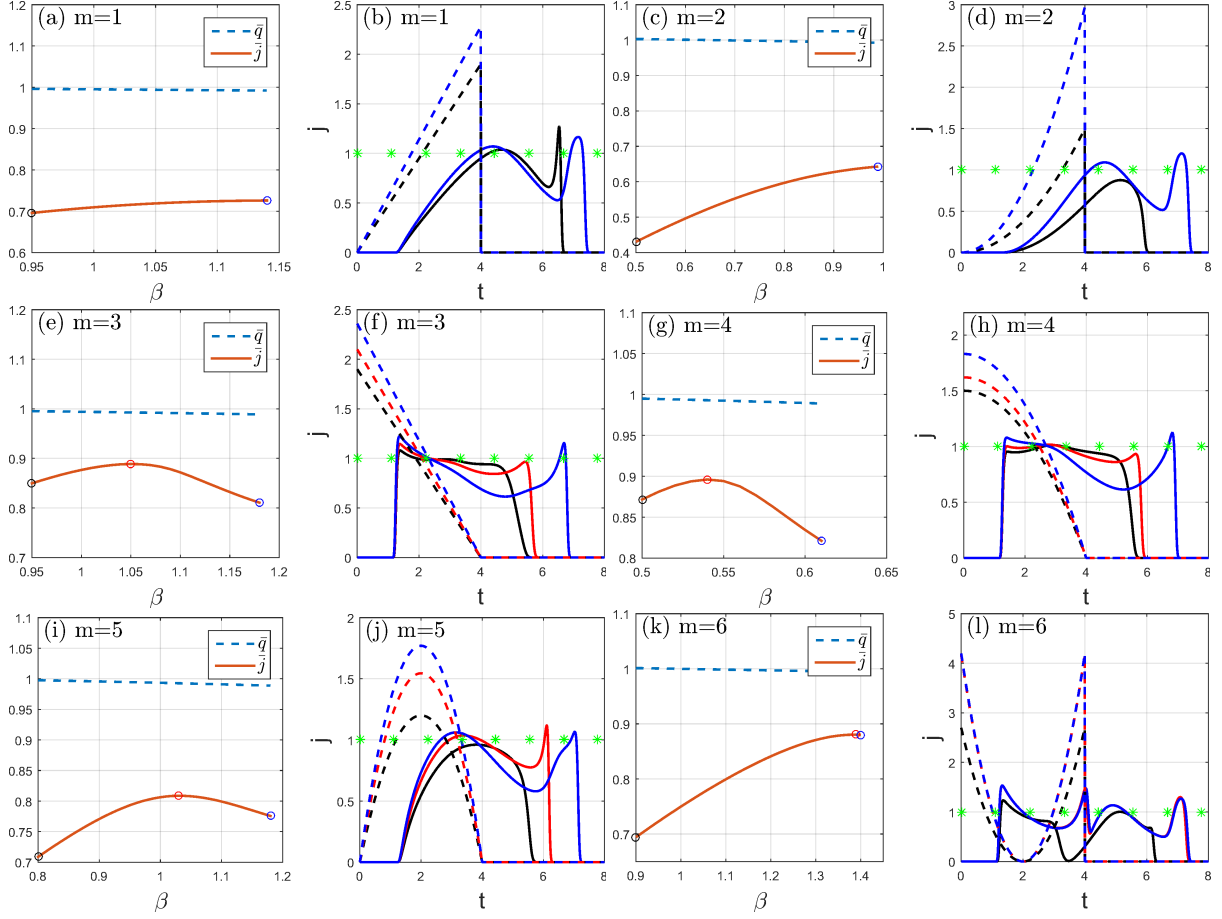


FIG. 3. (a, c, e, g, i, k) Scaled transmitted charge [cf. Eq. (20)], scaled current density [cf. Eq. (21)]. (b, d, f, h, j, l) Transmittance profiles at the anode for time-varying injection ones. Other marks are the same as Fig. 2. Parameters: $v_0 = \hat{c}/60$, $\tau_p = 4$, (a-b) $m = 1$; (c-d) $m = 2$; (e-f) $m = 3$; (g-h) $m = 4$; (i-j) $m = 5$; (k-l) $m = 6$.

relativistic effect becomes noticeable. When the injection is time-invariant with $v_0 = \hat{c}/60$, the transmittance goes below the known SC limit (see Fig. 4 (a-b)). Note again that they are scaled quantities following Ref.¹³, and all velocities are scaled with respect to L/T so light speed $\hat{c} = 30$. When the injection becomes time-varying ($m = 4$ and $v_0 = \hat{c}/60$ for example), the SC limit similarly clamps the transmittance profiles as Fig. 4 (c-d) shows. The SC limit also holds when initial velocity is changed to $v_0 = \hat{c}/10$ (see Fig. 4 (e-f)). Fig. 4 (b, d, f) shows the transmittance profiles become damped at the pulse trail when β_m increases. Note that \bar{q} becomes larger than unity because the charge density ρ becomes denser due to the relativistic factor (cf. $j_A = \rho_A v_A$ in Eq. (20)), and this increasing effect becomes less significant as the injection magnitude β_m increases (see

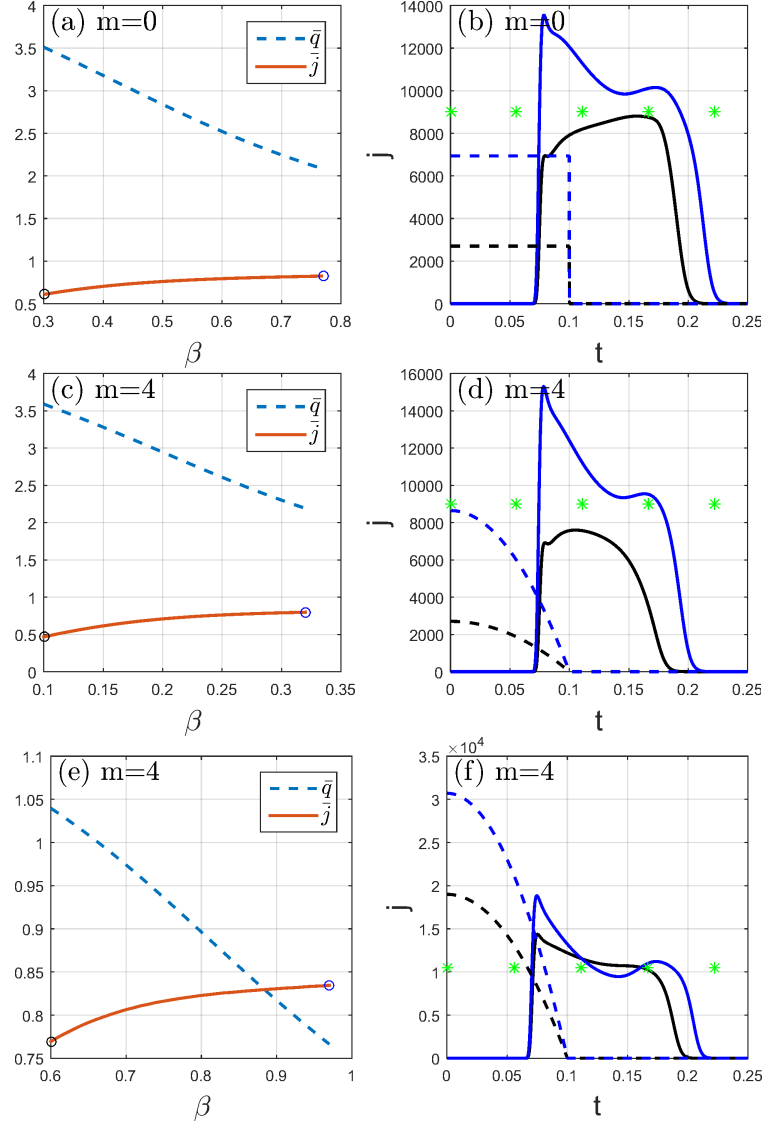


FIG. 4. (a, c, e) Scaled transmitted charge [cf. Eq. (20)] and scaled current density [cf. Eq. (21)]. (b, d, f) Transmittance profiles at anode for injection ones in relativistic regime ($m = 0, 4$). Other marks are the same as Fig. 2. Parameters: $\tau_p = 0.1$, $\phi_g = 900$. (a-b) $m = 0, v_0 = \hat{c}/60$; (c-d) $m = 4, v_0 = \hat{c}/60$; (e-f) $m = 4, v_0 = \hat{c}/10$.

Fig. 4 (a, c, e)).

C. Time-dependent quantities

More details can be observed from time-dependent plots of voltage potential $\phi(x, t)$ and charge density $\rho(x, t)$. Fig. 5 presents $\phi(x, t)$ and $\rho(x, t)$ at three instantaneous time points for a classical

case and a relativistic one in Fig. 5, when SC limit is reached respectively. We choose $t = 2.63$ and 0.053 to be the time when the injection current density become positive (cf. Figs. 3(g-h) and 4(c-d)) respectively. Fig. 5 shows that as the charge traverses the diode with time, the electric field at the cathode can become positive ($E_C = -\partial_x \phi$) and space charge accumulates near cathode to repel more electrons to emit. This is when SC limit dominates the electron flow process and the virtual diode forms. It is also speculated that the zero cathode field $E_C = 0$ is *not* a critical condition for space charge limit for time-varying injection cases, as previous work^{6,22} consider so. We speculate that time-dependent space-charge limit may involve more dynamic process of virtual cathode than a static zero cathode field. In our simulation, it is observed that virtual diode oscillation occurs when the scaled \bar{j} in Eq. (21) transcends unity. However, we do not include them in Sec. III because the SC limit is always reached when \bar{j} remains under unity.

D. Caveat: null emission velocity $v_0 = 0$

In the last example, we present the result of the special case when the emission velocity v_0 is zero. This example is compared with the time varying cases and serves as a validation case since this case is well understood theoretically. The inflow boundary condition Eq. (5) at $x = 0$ becomes

$$\phi = 0, \quad v = v_0, \quad \rho(t) = \beta_m \sigma_m(t), \quad 0 \leq t \leq \tau_p, \quad (22)$$

where β_m is also the dimensionless amplitude and $\sigma_m(t)$ the particular time-dependent profiles assumed for the inflow charge density. **Note that we apply a slightly different inflow boundary condition at $x = 0$. It is difficult to apply a boundary condition of a finite injection current density with a null emission velocity at $x = 0$ in the current model. For such a case, a kinetic model may be necessary to understand its limited current density.** The same outflow boundary condition $\phi = \phi_g$ applies as in the nonzero injection velocity case. The particular profiles $\sigma_m(t)$ are assumed to be polynomial for the same reason as the injection current densities $j_m(t)$ in Eqs. (8-14). This is the slightly different inflow boundary condition we apply in this subsection. Similar to Figs. 4, we present a result in Fig. 6 for $v_0 = 0, \rho_5(t) = \beta_5 \sigma_5(t)$ as the inflow boundary condition, because this represents a reasonable injection current density in pragmatic situations. First in Fig. 6(a), as β_5 increases, the scaled current density increases until 89% of the SC limit (cf. blue circle) and most charge remains in the diode spacing at the time of τ_p (cf. $\bar{q} \ll 1$ on the left axis). Second at $\beta_5 = 10.6$, the transmittance profile is distorted to the most extent (see Fig. 6(b)) due to SC effect.

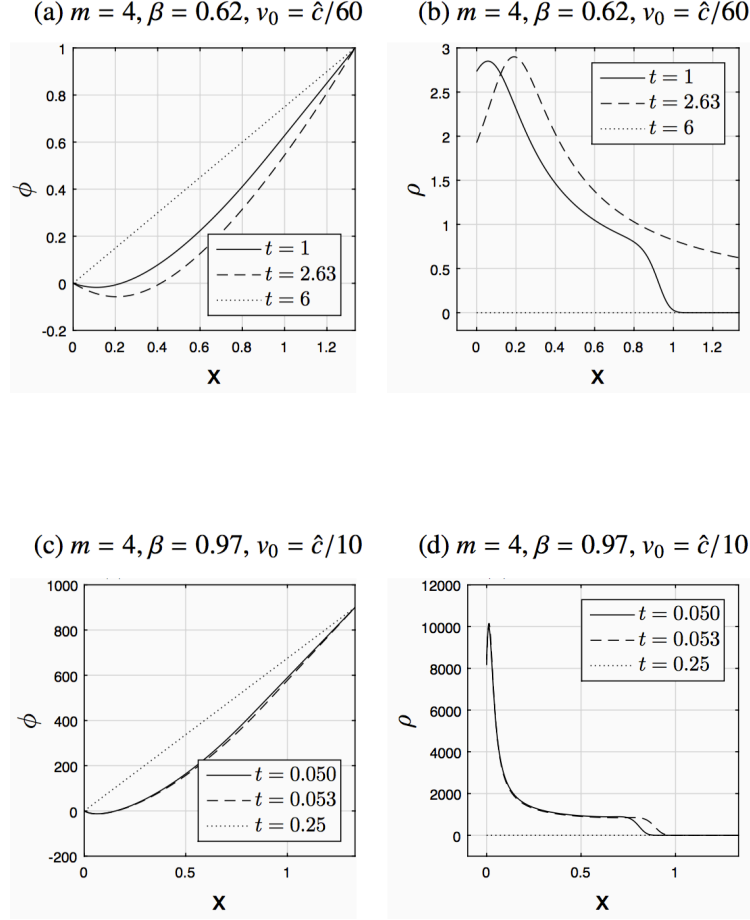


FIG. 5. Electric potential $\phi(x, t)$ and charge density $\rho(x, t)$ for classical and relativistic cases. Parameters: $m = 4$. Classical: (a-b) $\beta_4 = 0.62, v_0 = \hat{c}/60, \phi_g = 1$; relativistic: (c-d) $\beta_4 = 0.97, v_0 = 0.1\hat{c}, \phi_g = 900$.

Then we show that our simulation also treats the null-velocity case for the time-dependent charge in-flow.

IV. CONCLUSION

In summary, this paper addresses the question whether time-varying injection from cathode can push a transmitted current density through anode more than the conventional SC limit. Note that in our paper the injection beam is assumed to be cold and possesses no thermal spread at any instant in time for simplicity^{3,30}. From our simulations based on the 1D pressureless Euler-Poisson

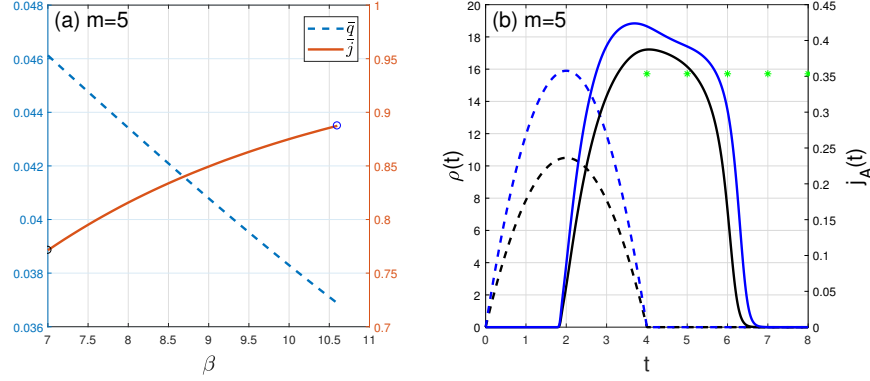


FIG. 6. (a) Scaled transmitted charge [cf. Eq. (20)] and scaled current density [cf. Eq. (21)]. (b) Injection charge density $\rho(t)$ (dashed curves) and transmittance profiles at anode $j_A(t)$ (solid curves). Note the curves in (a-b) are plotted in different scales labeled on the left and right sides of the line graph. Other marks are the same as Fig. 2. Parameters: $m = 5, \tau_p = 4, v_0 = 0, \phi_g = 1$. [Associated dataset available at <http://dx.doi.org/10.5281/zenodo.836163>]²⁹

equations, we speculate that the answer is *negative* under the condition of a fixed voltage difference across the diode. We also extend the classical diode to relativistic regime when initial velocity of electrons is close to the speed of light or when the diode voltage contributes to relativistic acceleration.

ACKNOWLEDGMENTS

L. Y. was supported by travel grant of Hangzhou Dianzi University [JGB06205-2017031] and UK EPSRC [grant number EP/I034548/1]. He owes the starting idea of time-dependent space-charge effect from L. K. Ang and thanks Lang Jiandong for useful discussion. Q. T. is supported by Eliza Ricketts Postdoctoral Fellowship.

Appendix A: Detailed derivation of relativistic extension for 1D electron flow

In this section, we start from the full relativistic formulation for the same 1D electron flow problem in Sec. II, using covariant four-vector³¹ and then simplify it to a new differential equations system, Eqs. (16), (17) and (18) therein. There can be many relativistic versions of our problem, for instance see Ref.³². We choose to formulate in a simple way to be reducible to classical regime when $v \ll c$.

We use four-vector in SI units (instead of natural units as convention) to represent every vectorial physical quantity in contra-variant components but the final main equations will be scaled under the same scaling of Eq. (4). Hence, the classical current density j , vector potential \mathbf{A} and static field E_x are replaced by four current \mathcal{J}^μ , four potential A^α , the electromagnetic tensor $F^{\alpha\beta}$ respectively with the metric tensor $g^{\mu\nu}$ and four velocity U being used. The detailed definitions are given as

$$\mathcal{J}^\mu = (c\rho, \mathbf{j}), \quad (\text{A1})$$

$$A^\alpha = \left(\frac{\phi}{c}, \mathbf{A}\right). \quad (\text{A2})$$

$$\partial^\nu := \left(\frac{\partial}{c\partial t}, -\nabla\right), \quad (\text{A3})$$

$$\partial_\nu := \left(\frac{\partial}{c\partial t}, \nabla\right), \quad (\text{A4})$$

$$F^{\alpha\beta} = \partial^\alpha A^\beta - \partial^\beta A^\alpha = \begin{pmatrix} 0 & -E_x/c & -E_y/c & -E_z/c \\ E_x/c & 0 & -B_z & B_y \\ E_y/c & B_z & 0 & -B_x \\ E_z/c & -B_y & B_x & 0 \end{pmatrix}, \quad (\text{A5})$$

$$g^{\mu\nu} = \text{diag}(1, -1, -1, -1). \quad (\text{A6})$$

$$U^\alpha = \gamma(c, \mathbf{v}), \quad (\text{A7})$$

$$U_\alpha = \gamma(c, -\mathbf{v}). \quad (\text{A8})$$

Therefore, the covariant formulation for the electron flow problem in the three equations³³ is written as

$$\partial_\mu \mathcal{J}^\mu = 0, \quad (\text{A9})$$

$$\frac{dU^\alpha}{d\tau} = \frac{q}{m} F^{\alpha\beta} U_\beta, \quad (\text{A10})$$

$$\partial_\alpha F^{\alpha\beta} = \mu_0 \mathcal{J}^\beta \quad (\text{A11})$$

We choose Coulomb gauge so that Poisson equation remains unchanged³⁴

$$\nabla^2 \phi = \frac{\rho(x, t)}{\epsilon_0}, \quad (\text{A12})$$

$$(\nabla^2 - \frac{1}{c^2} \partial_t^2) \mathbf{A} = -\mu_0 \mathbf{j}_t. \quad (\text{A13})$$

Since only 1D situation is considered, $\mathbf{j} = \hat{x}j$ and $\nabla \times \mathbf{j} = 0$ means the transverse current vanishes $j_t = 0$ ³⁴. It is legitimate to choose

$$\mathbf{A} = 0. \quad (\text{A14})$$

Then the magnetic field also vanishes, which is consistent with that 1D time-dependent electric field induces no magnetic field from Faraday's law of induction³⁴. Eq. (A10) leads to

$$\frac{d(\gamma v)}{\gamma d\tau} = \frac{q}{mc} (-\partial_x \phi) c = \frac{q}{m} F^{10} c = \frac{q}{m} E_x. \quad (\text{A15})$$

It is noted that the equation Eq. (A15) differs from $\gamma \partial_t v = qE_x/m$. From Eq. (A15) and $\gamma d\tau = dt$ we have the scaled relativistic dynamical equation [cf. Eq. (4)] as

$$\frac{d}{dt} [\gamma(v) \cdot v(x, t)] = \partial_x \phi, \quad (\text{A16})$$

which is expanded as

$$\gamma^3 \frac{d}{dt} v(x, t) = \partial_x \phi. \quad (\text{A17})$$

The sign appears reverse because of the negative sign of q . Eqs. (A9), (A17) and (A12) can be written as Eqs. (16), (17) and (18) \square .

REFERENCES

- ¹C. D. Child, Phys. Rev. **32**, 0492 (1911).
- ²I. Langmuir, Phys. Rev. **2**, 450 (1913).
- ³P. Zhang, A. Valfells, L. K. Ang, J. W. Luginsland, and Y. Y. Lau, [Applied Physics Reviews](#) **4**, 011304 (2017).
- ⁴G. Jaffé, [Phys. Rev.](#) **65**, 91 (1944).
- ⁵S. Liu and R. A. Dougal, [Journal of Applied Physics](#) **78**, 5919 (1995).
- ⁶H. R. Jory, [Journal of Applied Physics](#) **40**, 3924 (1969).
- ⁷W. L. Howes, [Journal of Applied Physics](#) **37**, 438 (1966).
- ⁸Y. Feng and J. P. Verboncoeur, [Phys. Plasmas](#) **15**, 112101 (2008).

- ⁹P. A. Lindsay, D. Li, and X. Chen, *Phys. Plasmas* **16**, 073303 (2009).
- ¹⁰Y. L. Liu, S. H. Chen, W. S. Koh, and L. K. Ang, *Phys. Plasmas* **21**, 043101 (2014).
- ¹¹J. W. Luginsland, Y. Y. Lau, R. J. Umstadtd, and J. J. Watrous, *Phys. Plasmas* **9**, 2371 (2002).
- ¹²R. Kumar and D. Biswas, *Phys. Plasmas* **15**, 023101 (2008).
- ¹³R. E. Caflisch and M. S. Rosin, *Physical Review E* **85** (2012), 10.1103/PhysRevE.85.056408.
- ¹⁴M. E. Griswold, N. J. Fisch, and J. S. Wurtele, *Phys. Plasmas* **17**, 114503 (2010).
- ¹⁵Y. Zhu and L. K. Ang, *Appl. Phys. Lett.* **98**, 051502 (2011).
- ¹⁶M. E. Griswold, N. J. Fisch, and J. S. Wurtele, *Phys. Plasmas* **19**, 024502 (2012).
- ¹⁷Y. Liu and L. K. Ang, in *The 39th IEEE International Conference on Plasma Science*, Session 3P: Computational Plasma Physics (poster session 2) (2012) pp. 3P–36.
- ¹⁸M. Pant and L. K. Ang, *Phys. Rev. B* **88** (2013), 10.1103/PhysRevB.88.195434.
- ¹⁹Y. Liu and L. K. Ang, *Journal of Physics D: Applied Physics* **47**, 125502 (2014).
- ²⁰Y. Liu, *Time-Varying Emission of Electrons and Its Relevant EM Phenomenon*, Ph.D. thesis (2014).
- ²¹M. E. Griswold and N. J. Fisch, *Phys. Plasmas* **23**, 014502 (2016).
- ²²Y. L. Liu, P. Zhang, S. H. Chen, and L. K. Ang, *Phys. Plasmas* **22**, 084504 (2015).
- ²³Y. Zhang, G. Liu, Z. Yang, Q. Xing, H. Shao, R. Xiao, H. Zhong, and Y. Lin, *Phys. Plasmas* **16**, 044511 (2009).
- ²⁴S. H. Chen, L. C. Tai, Y. L. Liu, L. K. Ang, and W. S. Koh, *Phys. Plasmas* **18**, 023105 (2011).
- ²⁵In 1D case, the current density j are simply related to the current J : $j = J/A$ where A is the area.
- ²⁶The increasing profiles (8-10) are normalised so that within the emission pulses they give the same account of charge $\int_0^{\tau_p} j_m(t)dt = \int_0^{\tau_p} 1dt = \tau_p$ and the other profiles are chosen to be as smoothly-varying as possible.
- ²⁷Á. Valfells, D. W. Feldman, M. Virgo, P. G. O’Shea, and Y. Y. Lau, *Phys. Plasmas* **9**, 2377 (2002).
- ²⁸B. Schutz, *A First Course in General Relativity*, 2nd ed. (Cambridge University Press, Beijing, 2011).
- ²⁹Y. Liu, *Zenodo* (2017), <http://dx.doi.org/10.5281/zenodo.836163>.
- ³⁰Y. Lau, *Phys. Rev. Lett.* **87** (2001), 10.1103/PhysRevLett.87.278301.
- ³¹L. D. Landau and E. M. Lifshitz, *The Classical Theory of Fields*, fourth revised english edition ed., Course of Theoretical Physics, Vol. 2 (Elsevier, Butterworth Heinemann, 1975).
- ³²W. H. Chan, S. Wong, and M. Yuen, *Journal of Mathematical Analysis and Applications* **439**,

925 (2016).

³³Note that the proper time τ is operated in full differential, instead of partial differential because τ is frame-independent for a certain particle.

³⁴J. D. Jackson, *Classical electrodynamics*, 3rd ed. (Wiley, New York, 1999).